

**Switching the perpendicular magnetization of a magnetic insulator by magnon transfer torque**C. Y. Guo,<sup>1,2,\*</sup> C. H. Wan,<sup>1,3,\*</sup> M. K. Zhao,<sup>1</sup> C. Fang,<sup>1</sup> T. Y. Ma<sup>①</sup>,<sup>1</sup> X. Wang,<sup>1</sup> Z. R. Yan,<sup>1</sup> W. Q. He,<sup>1</sup> Y. W. Xing,<sup>1</sup> J. F. Feng,<sup>1</sup> and X. F. Han<sup>①</sup>,<sup>1,2,3,†</sup><sup>1</sup>*Beijing National Laboratory for Condensed Matter Physics, Institute of Physics, University of Chinese Academy of Sciences, Chinese Academy of Sciences, Beijing 100190, China*<sup>2</sup>*Center of Materials Science and Optoelectronics Engineering, University of Chinese Academy of Sciences, Beijing 100049, China*<sup>3</sup>*Songshan Lake Materials Laboratory, Dongguan, Guangdong 523808, China* (Received 11 March 2021; revised 24 August 2021; accepted 24 August 2021; published 7 September 2021)

Magnon transfer torque (MTT) is regarded as capable of manipulating spin by magnons or spin waves only without spatial movement of electrons, which is a key to enrich the toolbox for magnonics. Here using a magnon current through an antiferromagnetic NiO spacer, which can be deep into a magnetic insulator  $\text{Y}_3\text{Fe}_5\text{O}_{12}$  (YIG), we demonstrated the perpendicular magnetization of the YIG in a YIG/NiO/Pt heterostructure could be switched. When the thickness of the magnon channel NiO was 1.5 nm, the magnon current could still maintain about 84% of the spin current for the YIG/Pt control device, indicating high efficiency of the NiO spacer in transferring magnon torque. Switching the perpendicular magnetization in the YIG/NiO/Pt heterostructures unambiguously verified the effect of magnon transfer torque (MTT), which may advance the development of magnonic memories and logics.

DOI: [10.1103/PhysRevB.104.094412](https://doi.org/10.1103/PhysRevB.104.094412)**I. INTRODUCTION**

Magnonics, which utilizes magnons to generate, transfer, control, and detect data without charge movement, emerges as a potential green electronics [1]. Owing to no interactions between magnons and conductive electrons, magnetic insulators such as  $\text{Y}_3\text{Fe}_5\text{O}_{12}$  (YIG) have longer spin relaxation length and lifetime [2] than magnetic metals, thus ideal to be implemented in magnonics [3–12]. However, also due to their insulating nature, there are only two ways to electrically control spins in magnetic insulators. One is using interfacial exchange coupling between localized spins in a magnetic insulator and delocalized electron spins in an adjacent metal [13]. The perpendicular magnetization of  $\text{Tm}_3\text{Fe}_5\text{O}_{12}$  or YIG has been switched [14,15] and the ultrahigh speed domain wall motion has also been driven [16] via spin Hall effect of a heavy metal in this way. Another possibility is using magnon current, which is still allowed inside a magnetic insulator and as-induced magnon transfer torque (MTT).

Here in a perpendicular YIG/NiO/Pt heterostructure, we demonstrate that the magnon current filtered by an insulating NiO layer can switch the perpendicular magnetization of the insulating YIG film. Thanks to the perpendicular magnetic anisotropy (PMA) of the YIG and the insulating nature of both YIG and NiO, our demonstration can be safely free from the mechanisms due to the Oersted field or tunneling spin current, which unambiguously confirms existence of the MTT effect.

**II. MATERIALS AND METHODS**

YIG films were deposited on  $\text{Y}_3\text{Sc}_2\text{Ga}_3\text{O}_{12}$  (YSGG) substrates using a magnetron sputtering system (ULVAC-MPS-

4000-HC7) with base vacuum of  $1 \times 10^{-6}$  Pa. An *ex situ* high-temperature annealing in the oxygen atmosphere was carried out to further improve the PMA, which originated from the lattice mismatch between YSGG and YIG and as-induced magnetoelastic energy [15]. The PMA was confirmed and measured by a physical property measurement system (PPMS-9T from Quantum Design) with a vibrating sample magnetometer (VSM) component. The NiO spacer ( $t = 0\text{--}25$  nm) and Pt (3.0 nm) top layer were deposited on the annealed YIG films in another high-vacuum magnetron sputtering chamber at room temperature. The YIG/NiO/Pt heterostructures were then patterned into the Hall bar devices with channel width of  $20 \mu\text{m}$  through standard ultraviolet photolithography and the following Ar ion etching. After the device microfabrication, transport experiments including the anomalous Hall effect and spin-Hall magnetoresistance were carried out with a Keithley 2400 applying current and a Keithley 2182 picking up voltage as shown in Fig. 1(b). A PPMS was used to provide magnetic field with the needed direction and to control the ambient temperature. Current induced magnetization switching was measured at 150 K. We applied the current pulse along the  $x$  axis with a duration of 50 ms and a period of 150 ms to activate spin dynamics. After each pulse, a small current was applied to pick up the Hall voltage along the  $y$  axis as shown in Fig. 1(b).

**III. RESULTS AND DISCUSSION****A. Structure of the YIG/NiO/Pt heterostructure**

Figure 1(a) shows structure of a YIG/NiO/Pt stack and the conversion process from a spin current into a magnon current at the Pt/NiO interface. When a charge current  $J_c$  flows through the Pt layer, a spin current  $J_s$  flowing along the film normal is then generated with polarization  $\sigma$  ori-

\*These authors contributed equally to this work.

†Corresponding author: xfhan@iphy.ac.cn

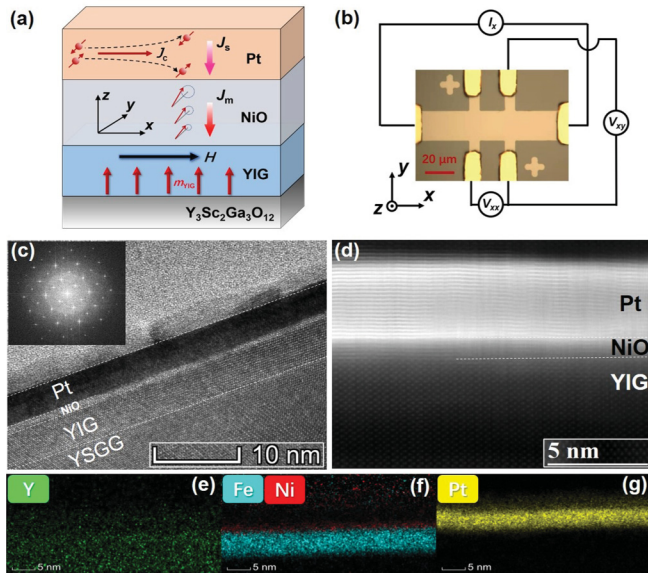


FIG. 1. Characterization of the perpendicular YIG/NiO/Pt structure. (a) Schematic diagram of the MTT effect in the structure. (b) Image of a patterned YIG(5.0)/NiO(1.5)/Pt(3.0 nm) Hall bar device. The current was applied along the  $x$  axis and the anomalous Hall voltage was picked up along the  $y$  axis. (c) The cross-sectional high-resolution TEM image of the YSGG//YIG(5.0)/NiO(1.5)/Pt(3.0 nm) structure. The inset shows the FFT pattern of the substrate. (d) The cross-sectional HAADF-STEM image of the same structure. [(e)–(g)] The corresponding energy dispersive x-ray (EDS) mapping of different elements.

entering along the  $y$  axis via the spin Hall effect [17]. The spin current flows toward the interface with NiO and results in the spin accumulation there. Due to the  $s$ - $d$  exchange

interaction at the Pt/NiO interface, extra magnons are created, which diffuse through NiO with a decaying ratio. Once reaching the bottom YIG, magnons are absorbed and then exert torque on local spins of the YIG and finally switch its magnetization.

Figure 1(b) shows measurement setups. The structure has been patterned into the Hall bar devices with a  $20\text{-}\mu\text{m}$  channel width. The high-resolution cross-sectional transmission electron microscopy (HRTEM by Titan Themis) was used to observe the YIG(5.0)/NiO(1.5)/Pt(3.0 nm) structure. The three layers were all continuous and flat. The interfaces of NiO/YIG and NiO/Pt were both clear and sharp. No pinholes were detected inside NiO [Fig. 1(c)]. Other regions showed similar film and interfacial quality. The high angle annular dark field (HAADF) image of the structure in Fig. 1(d) confirmed the HRTEM results. The HAADF image also showed good epitaxial growth of YIG on the YSGG substrate. Moreover, the two interfaces were atomically sharp [Fig. 1(d)]. The x-ray energy dispersion spectroscopy (EDS) mapping in Figs. 1(e)–1(g) correctly shows distribution of the Y, Fe, Ni, and Pt elements along the film normal, though low spatial resolution of the EDS could not reflect a clear NiO/Pt interface in Figs. 1(f) and 1(g) as the HAADF did. We also ensured the insulating nature of the NiO spacer.

The normalized  $M$ - $H$  curves of the stack measured by vibrating sample magnetometer (VSM) is shown in Fig. 2(a). The PMA was clearly built in the YIG film whose effective anisotropy field  $H_k$  was approximately 1580 Oe. The saturated magnetization and coercivity  $H_c$  were about 91.3 emu/cc and 10 Oe, respectively, all similar to Ref. [15]. Owing to the spin Hall magnetoresistance (SMR) effect and a nonzero imaginary part of spin-mixing conductance at the interface [18,19], The Hall resistance  $R_{xy}$  of Pt on the top of YIG/NiO could be detected. This phenomenon behaved similar to the anomalous

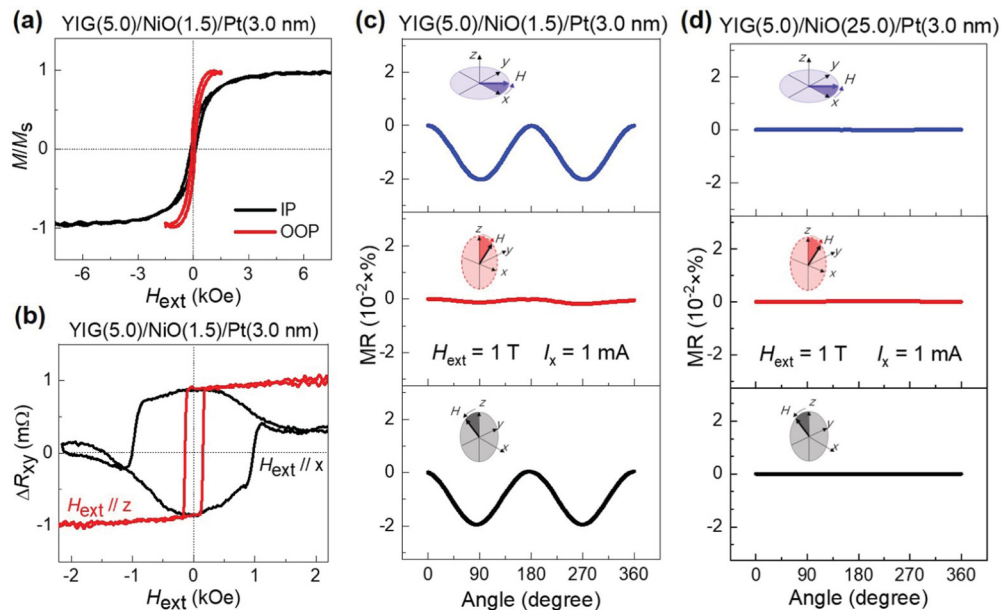


FIG. 2. AHE and SMR of the YIG/NiO/Pt structure. (a) In-plane and out-of-plane magnetic hysteresis loops of the YSGG//YIG(5.0)/NiO(1.5)/Pt(3.0 nm) structure measured by VSM at 150 K. (b) Anomalous Hall resistance of the YSGG//YIG(5.0)/NiO(1.5)/Pt(3.0 nm) Hall bar device as a function of the out-of-plane ( $H_z$ ) and in-plane magnetic field ( $H_x$ ). [(c) and (d)] Angular dependence of magnetoresistance of the YIG(5.0)/NiO(1.5)/Pt(3.0 nm) and the YIG(5.0)/NiO(25)/Pt(3.0 nm) structures, respectively. The illustrations in (d) correspond to definitions of different angles. All data were measured at 150 K.

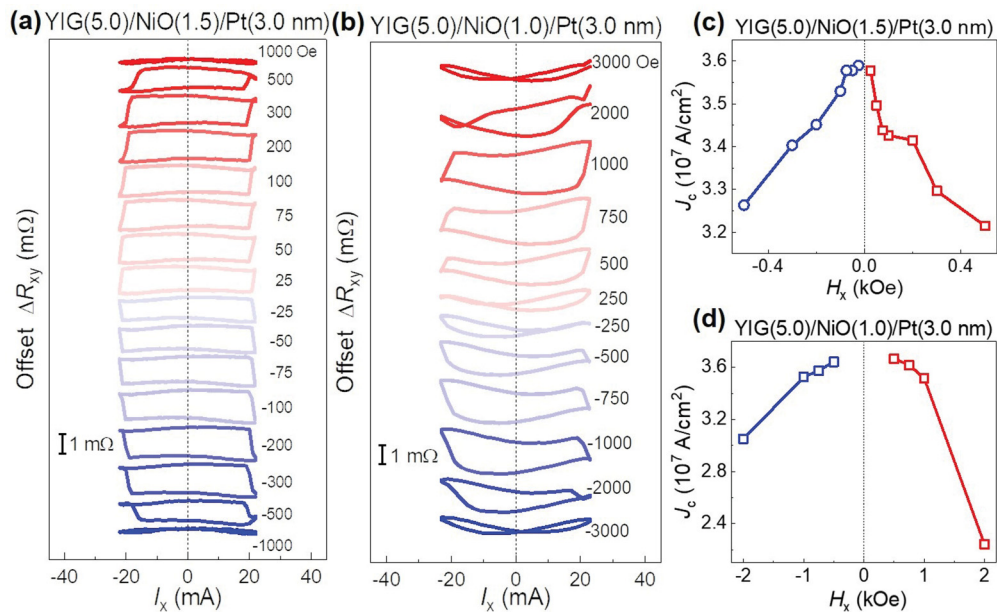


FIG. 3. Perpendicular magnetization switching driven by MTT in the perpendicular YIG/NiO/Pt structure. [(a) and (b)] The dependence of  $R_{xy}$  on switching current for YIG(5.0)/NiO(1.5)/Pt(3.0 nm) and YIG(5.0)/NiO(1.0)/Pt(3.0 nm), respectively, under different bias fields  $H_x$ . [(c) and (d)] The dependence of the critical switching current on  $H_x$  for the two devices ( $t_{NiO} = 1.5$  and 1.0 nm). All data were measured at 150 K.

Hall effect, which was used to mark the  $z$  component of magnetization as reported in Refs. [14,15]. The field dependence of  $R_{xy}$  in Fig. 2(b) also confirmed the well-established PMA. The obtained  $H_k$  was about 1620 Oe, coinciding with the VSM result. Figure 2(c) shows the angular dependencies of longitudinal resistance  $R_{xx}$  of the device with 1.5-nm NiO spacer. The 1-T field larger than  $H_k$  was applied to ensure the collinear YIG magnetization with the field. The magnetization was then rotated in the  $x$ - $y$ ,  $y$ - $z$ , and  $z$ - $x$  planes by the field. Meanwhile  $R_{xx}$  was measured and its variation  $\Delta R_{xx}$  with different angles is shown in Fig. 2(c).

### B. Magnetoresistance and as-induced anomalous Hall effect of the YIG/NiO/Pt structure

$\Delta R_{xx}$  dominantly changed in the  $x$ - $y$  and  $y$ - $z$  planes. Their magnetoresistance ( $MR = \Delta R_{xx}/R_{xx}$ ) were 0.0202% and 0.0195%, close to each other. Nearly the same (zero)  $\Delta R_{xx}$  in the  $x$ - $y$  and  $y$ - $z$  planes (the  $z$ - $x$  plane) coincided with the SMR scenario [18,19]: as the magnetization of YIG fixed in the  $z$ - $x$  plane and orthogonal to the spin polarization  $\sigma$  along the  $y$  axis in the Pt film, spin-transfer from Pt to YIG can always occur and then resistance of Pt is not changed; otherwise, the resistance oscillates between high and low states as the magnetization set perpendicularly and collinearly with the spin polarization, respectively. Thus SMR [Fig. 2(c)] also hinted on the nonlocal spin transfer between Pt and YIG. We have used a control device with 25-nm NiO spacer for the same SMR measurement. No SMR was found [Fig. 2(d)]. According to our experiment, the magnon diffusion length of NiO on YIG was about 3–4 nm [11]. Thick NiO blocked magnon transfer into YIG and therefore SMR was absent for the control sample.

### C. SOT-driven magnetization switching

Hereafter we measured the SOT (i.e., MTT)-driven magnetization switching for the YIG/NiO/Pt Hall bar devices. A field  $H_x$  was applied along the longitudinal direction of the Hall bar. The Hall resistance  $\Delta R_{xy}$  was used to monitor the perpendicular magnetization  $m_z$  of YIG. In the presence of the NiO spacer [Figs. 3(a) and 3(b)], the YIG magnetization could still be reversed between spin-up and spin-down states under positive and negative currents at positive  $H_x$  and 150 K. The positive (negative)  $H_x$  determined the switching direction as counterclockwise (clockwise), typical for SOT-driven switching of PMA films [14,15,17]. This SOT-switching behavior cannot be dominated by the Oersted field caused by the current because an in-plane Oersted field cannot break symmetry of a PMA system and achieve its deterministic switching. Furthermore, the switching direction (clockwise and counterclockwise) of the current dependence of magnetization was only determined by the symmetry-breaking field  $H_x$ , which is a symbolic feature for the type- $z$  SOT switching scheme [20] and has been used as a strong sign to evidence the spin transfer torque (STT) effect in Ref. [17]. Here we used this phenomenon as a mark to verify the MTT effect. The critical current density for the above two samples are summarized in Figs. 3(c) and 3(d). Typically,  $J_c$  of YIG/NiO(1.5 nm)/Pt was about  $3.6 \times 10^7$  A/cm $^2$  at  $H_x = 25$  Oe, comparable with  $J_c$  of  $1.7 \times 10^7$  A/cm $^2$  at  $H_x = 500$  Oe in the TIG/Pt system [14] and  $3.0 \times 10^7$  A/cm $^2$  at  $H_x = 50$  Oe in the YIG/Pt system [15]. Their variety may come from the difference in the perpendicular anisotropy energy, spin-transfer efficiency, or spin Hall angles.

Noticeably, NiO was chosen as a spacer to convert the electronic spin current into magnon current because of its high efficiency in transiting magnons [21,22] and to isolate

direct interaction between YIG and Pt. Owing to these characteristics of NiO, Wang *et al.* experimentally switched the magnetization of a permalloy film in a Bi<sub>2</sub>Se<sub>3</sub>/NiO/NiFe structure at room temperature [23]. The NiFe has in-plane magnetic anisotropy. In this case, cautions were taken to exclude the Oersted mechanism whose potential dominance in the magnetization switching process could nevertheless be safely ruled out here.

Besides pulse duration of 50 ms, we have also tried other pulse durations within the limitation of Keithley 2400 current source. No noticeable difference was observed. In the SOT switching measurement, a large current of 22 mA was used, which could elevate the device temperature by Joule heating. However, an increase in temperature alone cannot realize the deterministic switching of a perpendicular magnetization either. Even the combined effect of Joule heating and the Oersted mechanism (generating an in-plane field) cannot be physically responsible for the deterministic perpendicular magnetization switching, which is an advantage of this perpendicular YIG/NiO/Pt system over an in-plane system in testing MTT effect.

Furthermore, the insulating nature of YIG and NiO can also rule out the spin-polarized electron tunneling effect [24,25] between Pt and the insulating magnet. If we use a ferromagnetic metal/NiO/heavy metal structure to verify MTT, the transfer of spin angular momentum across the spacer can still be mediated by a conventional electronic spin current because the materials on both sides of the NiO spacer are conductors and direct or indirect tunneling cannot be fully avoided. References [24,25] have shown an ordinary spin current could pass from one electrode to the other through a tunnel barrier of several nanometers. The insulating nature of both YIG and NiO eliminated this possibility. These advantages of the YIG/NiO/Pt system are beneficial for the verification of the MTT effect.

We have measured NiO blocking temperature  $T_b$  ( $\sim 175$  K) (see Fig. 4), which confirmed the antiferromagnetic nature of the NiO spacer. The exchange bias field of the YIG(5.0)/NiO(1.5)/Pt(3.0 nm) sample was obtained from the  $\Delta R_{xy}$ - $H_z$  curves for different temperatures (from 5 to 325 K) [Fig. 4(a)]. We first raised the magnetic field to 1 T at room temperature in PPMS via linear mode. The field was applied along the film normal. Then we reduced the temperature to 5 K. When the temperature was stabilized at 5 K, we then reduced the magnetic field to 0 Oe via the oscillate mode in order to minimize the remanence field of the superconducting magnet in the PPMS. We then began to measure the  $\Delta R_{xy}$ - $H_z$  curves under the elevated temperatures. The  $\Delta R_{xy}$  was measured at  $I_x = 1$  mA. From Fig. 4(b), one can see the blocking temperature is about 175–180 K. These data indicate the antiferromagnetic order of the NiO spacer which is beneficial for magnon transport. Worth noting that the YIG film is a compensated ferrimagnet with two sublattices of opposite magnetization orientations. At low temperatures, it experienced a crossover of the magnetization of the sublattices, which led to the changed switching directions in the  $\Delta R_{xy}$ - $H_z$  curves below 50 K and above 50 K. Above 75 K, one sublattice dominated  $M_S$  eventually. Further increase of the temperature resulted in the declining trend of the  $H_{ex}$ . At about 175–180 K,  $H_{ex}$  became zero. We then obtained

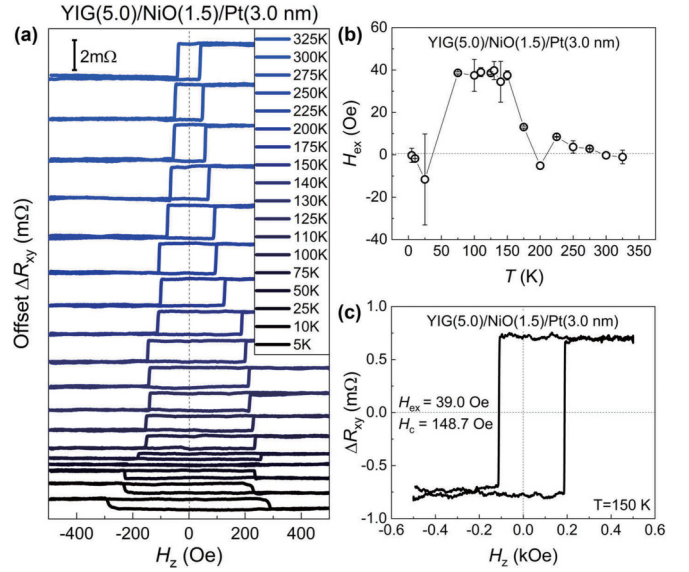


FIG. 4. Determination of the blocking temperature. (a)  $R_{xy}$ - $H_z$  curves at different temperatures vs the exchange bias. (b) Exchange bias field of the YIG(5.0)/NiO(1.5)/Pt(3.0 nm) obtained from the  $\Delta R_{xy}$ - $H_z$  curves for different temperatures in (a). (c)  $\Delta R_{xy}$ - $H_z$  curves of YIG(5.0)/NiO(1.5)/Pt(3.0 nm) under 150 K.

the blocking temperature  $\sim 175$  K of the device with 1.5-nm NiO. Especially, the exchange bias was maintained at 150 K [Fig. 4(c)], indicating that the antiferromagnetic nature of YIG can be kept at the temperature at which SOT-switching measurement has been conducted.

Efficient magnon current transmission across NiO relies on its antiferromagnetism or spin correlation [21,22], which requires the ambient temperature ( $T$ ) to be below or near its Néel temperature. On the other hand, when  $T$  was too low, magnons were quenched and the magnon conductance in NiO was low. Therefore we only achieved the magnetization reversal via MTT around 150–200 K for  $t_{NiO} = 1.5$  nm, indicating that magnons played a role in the transferring of the magnon angular momentum.

The critical switching current (density) was about 21 mA ( $3.51 \times 10^7$  A/cm<sup>2</sup>) at  $H_x = 100$  Oe [Fig. 3(a)]. Using this critical switching density  $J_c$ , we evaluated efficiency  $\eta$  of MTT cross the NiO spacer or effective spin Hall angle  $\theta_{SH}^{eff}$ , following Eq. (1) [26]:

$$\theta_{SH}^{eff} = \eta \theta_{SH} = \frac{e M_S t_F}{\hbar J_c} \left( \frac{H_k}{2} - \frac{H_x}{\sqrt{2}} \right). \quad (1)$$

Here,  $e$  is the elementary charge,  $\hbar$  is the reduced Planck constant,  $J_c$  is the critical current density,  $H_x$  is the applied field,  $t_F$  is thickness of YIG, and  $\eta \theta_{SH}$  ( $\theta_{SH}^{eff}$ ) is the (effective) spin Hall angle of Pt.  $H_k = 1620$  Oe and  $M_S = 91.3$  emu/cc at 150 K.  $\theta_{SH}^{eff} = \eta \theta_{SH}$  for YIG/Pt and YIG/NiO(1.5)/Pt were about 0.032 and 0.027, respectively. Figure 5(b) shows the current dependence of  $\Delta R_{xy}$  for YIG/Pt. Assuming that Pt in this study shared the same  $\theta_{SH}$ , the difference in  $\eta \theta_{SH}$  then actually reflected the MTT efficiency  $\eta$  cross the NiO spacer. If  $\eta$  of YIG/Pt was 1, then  $\eta$  for the 1.5 nm NiO was about 0.84 at 150 K, indicating high efficiency of NiO in delivering magnon current.

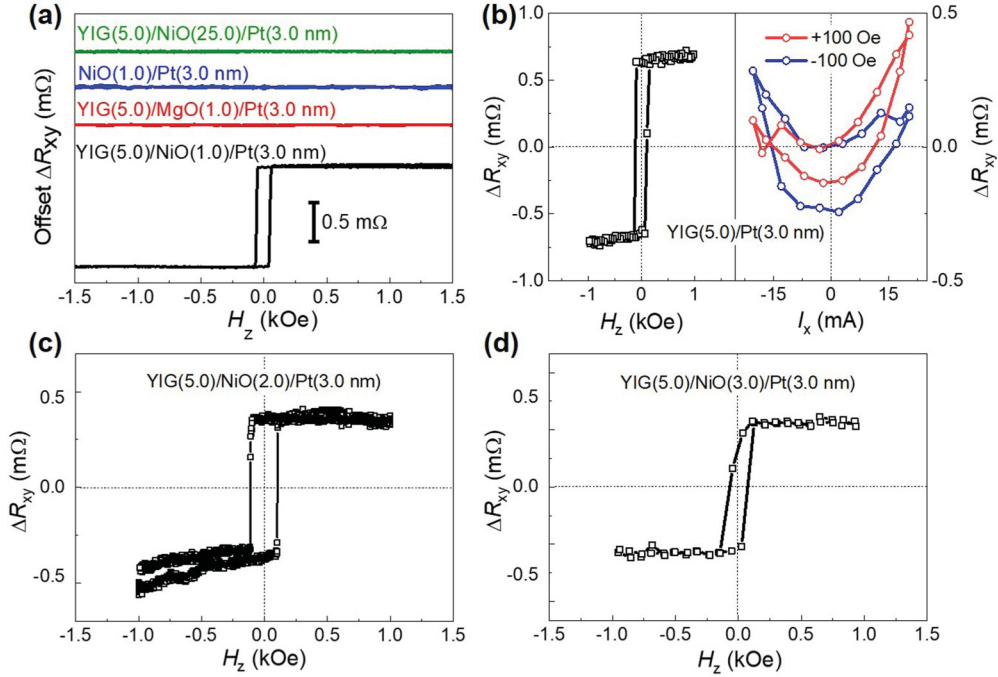


FIG. 5. AHE and MTT switching behaviors for different control samples. (a)  $\Delta R_{xy}$  measurements for the YIG/MgO(1.0 nm)/Pt, NiO(1.0 nm)/Pt, YIG/NiO(1.0 nm)/Pt, and YIG/NiO(25 nm)/Pt samples. [(b)–(d)] AHE and MTT-induced magnetization switching curves at  $H_x = 100$  Oe for the YIG/NiO( $t_{\text{NiO}}$ )/Pt samples with  $t_{\text{NiO}} = 0, 2.0,$  and  $3.0$  nm. Corresponding  $H_z$  dependence of  $\Delta R_{xy}$  are also shown. For  $t_{\text{NiO}} = 0$ , MTT switching was observed with  $H_x$  changing the switching direction on the basis of a parabolic background due to current-induced heating. For  $t_{\text{NiO}} = 2.0$  and  $3.0$  nm, AHE due to the SMR effect was observed. However, MTT switching was absent for the two samples. All data were measured at 150 K.

Spin dynamics driven by MTT can be described by Landau-Lifshitz-Gilbert equation:

$$\frac{\partial \mathbf{M}_f}{\partial t} = \mathbf{M}_f \times \mathbf{H} + \alpha \mathbf{M}_f \times \frac{\partial \mathbf{M}_f}{\partial t} + \boldsymbol{\tau}_{\text{MTT}}, \quad (2)$$

where  $\mathbf{M}_f$  is YIG magnetization,  $\mathbf{H}$  is the effective magnetic field including applied and anisotropy fields, and  $\alpha$  is the damping constant. Similar with STT [27,28], MTT can be expressed as  $\boldsymbol{\tau}_{\text{MTT}} = J_M P_g \mathbf{M}_f \times (\boldsymbol{\sigma} \times \mathbf{M}_f)$ , where  $J_M$  is the magnon current,  $P$  is the effective spin polarization of magnon current,  $g$  depends on the Néel vector of the AFM layer, and  $\boldsymbol{\sigma}$  is the unit vector of magnon polarization. MTT shares a similar form with the Slonczewski torque.

It is well-known that magnon decay in AFM is generic due to the energy dissipation caused by magnon-magnon and magnon-phonon coupling. So, the increase in the thickness of AFM leads to the decrease in  $J_M$ . The  $g$  value depends on spin configurations of AFM [29]. If the Néel vector of the AFM is perpendicular to the YIG magnetization, the magnon polarization becomes zero due to a magnon selection rule [29].  $J_M$  and  $g$  can thus be engineered in an AFM spacer to achieve a lower  $J_c$ .

Compared to the case of YIG/Pt, the decrease in  $\theta_{\text{SH}}^{\text{eff}}$  stemmed from the limited magnon conductance at the NiO/YIG interface and magnon relaxation in the NiO spacer. Furthermore, the interfacial magnon conductance can be influenced by the interfacial exchange coupling between NiO and YIG. Thus, to increase  $\theta_{\text{SH}}^{\text{eff}}$ , a strong interfacial exchange coupling between NiO and YIG and high quality of NiO are desired.

A series of control samples were designed to rule out other factors.  $\Delta R_{xy}$  of the control samples YSGG//YIG/MgO(1.0 nm)/Pt, YSGG//NiO(1.0 nm)/Pt, and YSGG//YIG/NiO(25 nm)/Pt were measured. In Fig. 5(a), except for the YIG/NiO(1.0 nm)/Pt sample, we have detected no anomalous Hall effect for the other control samples, which confirmed that the AHE originated from the SMR mechanism. Then, we tested switching behaviors for the YIG/NiO/Pt systems with different NiO thickness. We observed magnetization switching only when the NiO spacer was thin enough ( $t_{\text{NiO}} = 0$ – $1.5$  nm) [Figs. 5(b) and 3]. When the NiO thickness increased to 2.0, 3.0, and 25 nm, no switching behavior was observed. However, AHE was still observed for the device with  $t_{\text{NiO}} = 2.0$  and  $3.0$  nm [Figs. 5(c) and 5(d)], but it was not observed for the 25-nm sample. This feature indicated that MTT was still enabled for the device with  $t_{\text{NiO}} = 2.0$  and  $3.0$  nm, though their  $\eta$  was not large enough to realize MTT switching.

Worth noting, we have noticed the work of Wang *et al.* [23] in which magnons were reported to transfer torque across a 25-nm NiO spacer. In contrast, our result showed that only NiO thinner than 1.5 nm could transfer large enough MTT to switch the perpendicular YIG. The difference could probably result from different NiO quality grown on Bi<sub>2</sub>Se<sub>3</sub> and YIG. In our case, the magnon diffusion length was about 3.0–4.0 nm [11] while other values of 1–10 nm [21,22] were also reported before, depending on fabrication conditions, which might account for the aforementioned difference.

#### IV. CONCLUSION

In conclusion, MTT has been unambiguously demonstrated without contamination of the Oersted field mechanism and potential spin-polarized electron tunneling (i.e., STT effect) artifacts in this work. Furthermore, MTT is strong enough to switch the perpendicular magnetization of a magnetic insulator with  $H_k$  of 1.6 kOe. Compared with YIG/Pt, the NiO spacer, as a magnon median, could effectively retain the MTT efficiency at about 84% at 150 K as the NiO was thinner than 1.5 nm. Recently, the magnetization of a magnetic insulator has been demonstrated detectable by a so-called magnon-mediated nonlocal SMR effect [30]. Combined with this work, the demonstration of MTT in magnetic/antiferromagnetic insulators manifests the feasibility to design electrically controllable pure magnon devices such as magnonic memories and processors and to further advance the development of magnonics.

#### ACKNOWLEDGMENTS

This work was supported by the National Key Research and Development Program of China (MOST) (Grants No.

2017YFA0206200 and No. 2016YFA0300802), the National Natural Science Foundation of China (NSFC) (Grants No. 51831012, No. 51620105004, and No. 11974398), Beijing Natural Science Foundation (Grant No. Z201100004220006), the Strategic Priority Research Program (B) of Chinese Academy of Sciences (CAS) (Grant No. XDB33000000), and Foshan Science and Technology Innovation Team Project (FS0AA-KJ919-4402-0022). C.H. Wan appreciates the financial support from Youth Innovation Promotion Association, CAS (2020008). Dr. Zhang and Dr. Zheng from ZKKF (Beijing) Science & Technology Co., Ltd. are acknowledged for the HRTEM observations and analysis. We also thank Prmat (Shanghai) Technology Co., Ltd. for their offered YSGG substrates.

X.F.H. led and was involved in all aspects of the project. C.H.W. and C.Y.G. contributed equally to this work. C.Y.G., C.H.W., and M.K.Z deposited stacks and fabricated devices. C.Y.G., T.Y.M., and F.C. conducted magnetic and transport property measurements. C.H.W., C.Y.G., Z. R. Y., and X. W. contributed to the modeling and theoretical analysis. X.F.H., C.H.W., and C.Y.G. wrote the paper. X.F.H. and C.H.W. supervised and designed the experiments. All authors contributed to data mining and analysis.

- 
- [1] A. V. Chumak, V. I. Vasyuchka, A. A. Serga, and B. Hillebrands, Magnon spintronics, *Nat. Phys.* **11**, 453-461 (2015).
- [2] A. A. Serga, A. V. Chumak, and B. Hillebrands, YIG magnonics, *J. Phys. D: Appl. Phys.* **43**, 264002 (2010).
- [3] D. Qu, S. Y. Huang, Jun Hu, Ruqian Wu, and C. L. Chien, Intrinsic Spin Seebeck Effect in Au/YIG, *Phys. Rev. Lett.* **110**, 067206 (2013).
- [4] T. Kikkawa, K. Uchida, Y. Shiomi, Z. Qiu, D. Hou, D. Tian, H. Nakayama, X.-F. Jin, and E. Saitoh, Longitudinal Spin Seebeck Effect Free from the Proximity Nernst Effect, *Phys. Rev. Lett.* **110**, 067207 (2013).
- [5] E. Saitoh, M. Ueda, H. Miyajima, and G. Tatara, Conversion of spin current into charge current at room temperature: Inverse spin-Hall effect, *Appl. Phys. Lett.* **88**, 182509 (2006).
- [6] H. Wu, C. H. Wan, X. Zhang, Z. H. Yuan, Q. T. Zhang, J. Y. Qin, H. X. Wei, X. F. Han, and S. Zhang, Observation of magnon-mediated electric current drag at room temperature, *Phys. Rev. B* **93**, 060403(R) (2016).
- [7] J. Li, Y. Xu, M. Aldosary, C. Tang, Z. S. Lin, S. F. Zhang, R. Lake, and J. Shi, Observation of magnon-mediated current drag in Pt/yttrium iron garnet/Pt (Ta) trilayers, *Nat. Commun.* **7**, 10858 (2016).
- [8] H. Wu, L. Huang, C. Fang, B. S. Yang, C. H. Wan, G. Q. Yu, J. F. Feng, H. X. Wei, and X. F. Han, Magnon Valve Effect between Two Magnetic Insulators, *Phys. Rev. Lett.* **120**, 097205 (2018).
- [9] L. J. Cornelissen, J. Liu, B. J. Van Wees, and R. A. Duine, Spin-Current-Controlled Modulation of the Magnon Spin Conductance in a Three-Terminal Magnon Transistor, *Phys. Rev. Lett.* **120**, 097702 (2018).
- [10] J. Cramer, F. Fuhrmann, U. Ritzmann, V. Gall, T. Niizeki, R. Ramos, Z. Y. Qiu, D. Z. Hou, T. Kikkawa, J. Sinova, U. Nowak, E. Saitoh, and M. Kläui, Magnon detection using a ferroic collinear multilayer spin valve, *Nat. Commun.* **9**, 1089 (2018).
- [11] C. Y. Guo, C. H. Wan, X. Wang, C. Fang, P. Tang, W. J. Kong, M. K. Zhao, L. N. Jiang, B. S. Tao, G. Q. Yu, and X. F. Han, Magnon valves based on YIG/NiO/YIG all-insulating magnon junctions, *Phys. Rev. B* **98**, 134426 (2018).
- [12] K. Wright, Focus: A trio of magnon transistors, *Physics* **11**, 23 (2018).
- [13] S. S.-L. Zhang, and S. F. Zhang, Magnon Mediated Electric Current Drag across a Ferromagnetic Insulator Layer, *Phys. Rev. Lett.* **109**, 096603 (2012).
- [14] C. O. Avci, A. Quindeau, C. F. Pai, M. Mann, L. Caretta, A. S. Tang, M. C. Onbasli, C. A. Ross, and G. S. D. Beach, Current-induced switching in a magnetic insulator, *Nat. Mater.* **16**, 309 (2017).
- [15] C. Y. Guo, C. H. Wan, M. K. Zhao, H. Wu, C. Fang, Z. R. Yan, J. F. Feng, H. F. Liu, and X. F. Han, Spin-orbit torque switching in perpendicular  $Y_3Fe_5O_{12}$ /Pt bilayer, *Appl. Phys. Lett.* **114**, 192409 (2019).
- [16] L. Caretta, S.-H. Oh, T. Fakhru, D.-K. Lee, B. H. Lee, S. K. Kim, C. A. Ross, K.-J. Lee, and G. S. D. Beach, Relativistic kinematics of a magnetic soliton, *Science* **370**, 1438 (2020).
- [17] L. Liu, O. J. Lee, T. J. Gudmundsen, D. C. Ralph, and R. A. Buhrman, Current-Induced Switching of Perpendicularly Magnetized Magnetic Layers using Spin Torque from the Spin Hall Effect, *Phys. Rev. Lett.* **109**, 096602 (2012).
- [18] Y. T. Chen, S. Takahashi, H. Nakayama, M. Althammer, S. T. B. Goennenwein, E. Saitoh, and G. E. W. Bauer, Theory of spin Hall magnetoresistance, *Phys. Rev. B* **87**, 144411 (2013).
- [19] H. Nakayama, M. Althammer, Y. T. Chen, K. Uchida, Y. Kajiwara, D. Kikuchi, T. Ohtani, S. Geprägs, M. Opel, S. Takahashi, R. Gross, G. E. W. Bauer, S. T. B. Goennenwein, and E. Saitoh, Spin Hall Magnetoresistance Induced by a

- Nonequilibrium Proximity Effect, *Phys. Rev. Lett.* **110**, 206601 (2013).
- [20] S. Fukami, T. Anekawa, C. Zhang, and H. Ohno, A spin-orbit torque switching scheme with collinear magnetic easy axis and current configuration, *Nat. Nanotech.* **11**, 621 (2016).
- [21] H. Wang, C. Du, P. C. Hammel, and F. Y. Yang, Antiferromagnonic Spin Transport from  $\text{Y}_3\text{Fe}_5\text{O}_{12}$  into NiO, *Phys. Rev. Lett.* **113**, 097202 (2014).
- [22] W. Lin, K. Chen, S. Zhang, and C. L. Chien, Enhancement of Thermally Injected Spin Current through an Antiferromagnetic Insulator, *Phys. Rev. Lett.* **116**, 186601 (2016).
- [23] Y. Wang, D. Zhu, Y. Yang, K. Lee, R. Mishra, G. Go, S.-H. Oh, D.-H. Kim, K. M. Cai, E. L. Liu, S. D. Pollard, S. Y. Shi, J. M. Lee, K. L. Teo, Y. Wu, K.-J. Lee, and H. Yang, Magnetization switching by magnon-mediated spin torque through an antiferromagnetic insulator, *Science* **366**, 1125 (2019).
- [24] Y. Wang, R. Ramaswamy, M. Motapothula, K. Narayanapillai, D. P. Zhu, J. W. Yu, T. Venkatesan, and H. Yang, Room-temperature giant charge-to-spin conversion at the  $\text{SrTiO}_3$ - $\text{LaAlO}_3$  oxide interface, *Nano Lett.* **17**, 7659 (2017).
- [25] C. Cerqueira, J. Y. Qin, H. Dang, A. Djéffal, J.-C. Le Breton, M. Hehn, J.-C. Rojas-Sanchez, X. Devaux, S. Suire, S. Migot, P. Schieffer, J.-G. Mussot, P. Laczkowski, A. Anane, S. PetitWatelot, M. Stoffel, S. Mangin, Z. Liu, B. W. Cheng, X. F. Han, H. Jaffrès, J.-M. George *et al.*, Evidence of pure spin-current generated by spin pumping in interface-localized states in hybrid metal-silicon-metal vertical structures, *Nano Lett.* **19**, 90 (2018).
- [26] K. S. Lee, S. W. Lee, B. C. Min, and K.-J. Lee, Threshold current for switching of a perpendicular magnetic layer induced by spin Hall effect, *Appl. Phys. Lett.* **102**, 112410 (2013).
- [27] R. Cheng, D. Xiao, and J. G. Zhu, Antiferromagnet-based magnonic spin-transfer torque, *Phys. Rev. B* **98**, 020408(R) (2018).
- [28] Y. Cheng, K. Chen, and S. Zhang, Giant magneto-spin-Seebeck effect and magnon transfer torques in insulating spin valves, *Appl. Phys. Lett.* **112**, 052405 (2018).
- [29] Z. R. Yan, C. H. Wan, and X. F. Han, Magnon blocking effect in an antiferromagnet-spaced magnon junction, *Phys. Rev. Appl.* **14**, 044053 (2020).
- [30] C. Y. Guo, C. H. Wan, W. Q. He, M. K. Zhao, Z. R. Yan, Y. W. Xing, X. Wang, P. Tang, Y. Z. Liu, S. Zhang, Y. W. Liu, and X. F. Han, A nonlocal spin Hall magnetoresistance in a platinum layer deposited on a magnon junction, *Nat. Electron.* **3**, 304 (2020).